J. Fluid Mech. (1985), vol. 157, pp. 135–162
Printed in Great Britain

The transition to wavy Taylor vortices

By C. A. JONES
School of Mathematics, University of Newcastle-upon-Tyne, NE1 7RU

(Received 6 July 1984)

The transition from steady axisymmetric Taylor vortices to time-dependent wavy vortices is examined. The critical Taylor number and frequency at the transition point are determined in the infinite-cylinder approximation for a wide range of parameters. The results are compared with long-aspect-ratio experiments. The variation with axial wavelength is examined, and is found to be important when the radius ratio $\eta < 0.75$. A new spatially subharmonic mode is found to be the most unstable mode in some parameter regimes. This mode is identified with the jet mode recently discovered experimentally by Lorenzen, Pfister & Mullin and by Cole.

1. Introduction

The problem addressed in this paper is the transition to non-axisymmetric motion in the flow between rotating cylinders. There has been a considerable amount of experimental work done on Taylor–Couette flows in recent years, and the transition to three-dimensional motion has been considered by a number of authors. The experimental work to which the calculations described here are most relevant is reported in Cole (1981, 1983), Lorenzen, Pfister & Mullin (1982), Park (1984) and Park & Jeong (1984). Much of this new work has been directed to understanding the transition to three-dimensional time-dependent motion in wide-gap apparatus, which we define here as an apparatus having a radius ratio $\eta = R_{\text{inner}}/R_{\text{outer}} < 0.8$.

The transition from purely azimuthal Couette flow to axisymmetric motion was first discussed by Taylor (1923) and occurs at a value of the Reynolds number denoted by Re_c. The next transition to wavy Taylor vortices, occurring at a Reynolds number Re_w, was considered by Davey, DiPrima & Stuart (1968). These authors used weakly nonlinear theory, based on expansion in powers of the parameter $(Re - Re_c)$, which is assumed small. In earlier papers (Jones 1981, 1982) fully nonlinear Taylor-vortex flows were calculated numerically using spectral methods, and the stability of these solutions to wavy modes was also examined by using spectral methods. This work indicated that below $\eta = 0.8$ the stability boundary in the (Re, η)-plane occurs at a rapidly increasing Reynolds number. This rapid increase in Re when $0.75 < \eta < 0.8$ has been confirmed experimentally (e.g. Cole 1983). The experiments also indicate that a transition to wavy modes can exist even for radius ratios of order 0.5, but that the transition occurs at higher Reynolds numbers than it was possible to compute with the techniques used in Jones (1981). It was therefore decided to develop new numerical methods capable of reaching higher Reynolds numbers in order to compare with the recent experiments: the numerical techniques used for this work are described in Jones (1984). Most of the work done in this paper is concerned with radius ratios in the range $0.5 < \eta < 0.8$ and it is all based on the infinite-cylinder approximation; that is, we impose periodic boundary conditions in the z-direction.

Four aspects of the transition problem are considered here in detail. First, we

compare the theoretical 'infinite-cylinder' stability boundary with the experimentally determined finite-aspect-ratio results, and also compare the theoretical wave speeds with the actual ones. Secondly, we wish to investigate how this boundary varies with axial wavelength. Thirdly, we explore the new 'jet mode' of instability, observed by both Lorenzen *et al.* (1982) and Cole (1982); finally, we explore the physical mechanisms responsible for the very complicated behaviour of the wavy-vortex transition in the range $0.5 < \eta < 0.8$.

The experiments of Cole (1976) indicate that the critical Reynolds number for the onset of waves is strongly affected by end effects. Even for an aspect ratio $\Gamma = h/d$ (h being the height and d the gap in the apparatus) as great as 40 the onset of waves may occur at a Reynolds number measurably greater than that at larger aspect ratios. Nevertheless, his evidence suggested that, although the approach to the limit $\Gamma \to \infty$ was deferred to large values of Γ, such a limit exists. The experiments of Mullin & Benjamin (1980) and Lorenzen *et al.* (1982), working with aspect ratios generally lower than those of Cole, showed that in a wide-gap apparatus the critical value of Re can be an extremely sensitive function of aspect ratio, casting doubt even on the existence of a limit as $\Gamma \to \infty$; however, in their work the number of cells in the apparatus was kept constant as Γ was varied so that the size of the individual cells varied with Γ. In the infinite-cylinder theory, the wavelength is not determined, but is an input parameter. This makes it possible to explore the hypothesis that it is the variation in cell size which is responsible for the strong Γ sensitivity of the Mullin & Benjamin (1980) and Lorenzen *et al.* (1982) experiments.

Both Cole and Lorenzen *et al.* noted that for radius ratios around 0.5 a mode of instability appears that is radically different from the usual wavy mode of instability. The mode occurs preferentially for axial wavelengths shorter than square-cell values, and it has adjacent outflow boundaries moving in antiphase, rather than in phase. This suggests that the disturbance is periodic with an axial wavelength which is twice that of the mean flow. This mode is also observed to have its maximum amplitude in the region of the outflow boundary, hence its name, the jet mode. We investigate this mode here by means of the stability analysis of the axisymmetric Taylor vortices.

The physical mechanisms for the onset of wavy vortices are also considered in the light of the numerical calculations. Davey *et al.* (1968) took up a suggestion of Meyer (1966), that an important ingredient of the instability was the 'Orr–Sommerfeld' type of instability associated with the jet-like azimuthal flow in the neighbourhood of the inflow and outflow boundaries. We pursue this hypothesis in §4.

The basic difference between the work reported here and the amplitude-expansion methods of Davey *et al.* (1968) is that here the axisymmetric Taylor vortices are computed numerically by a fully two-dimensional calculation, whereas the amplitude expansions are based about the first critical Reynolds number Re_c and so involve only ordinary differential equations. The amplitude-expansion methods have been developed further, notably by Eagles (1971) and Di Prima, Eagles & Ng (1984). Although the predicted torque given by the amplitude expansions agrees rather well with both experiments and numerical calculations (Jones 1981) even at Reynolds numbers as high as $4Re_c$, the eigenvalue spectrum is not so faithfully represented. The turn-back of the $m = 1$ mode in the (Re, η)-plane is found, but the minimum value of η is near 0.6 (DiPrima *et al.* 1984), which is considerably lower than that observed experimentally. The region of the neutral curve where $m = 3$ is the most unstable mode is not found by amplitude-expansion methods; this is not surprising, of course, as the range of validity of these expansions is Re close to Re_c.

2. Specification of the problem

The formulation of the nonlinear Navier–Stokes equations used in these calculations has been described in detail in Jones (1984). Here we summarize so that the notation used in subsequent sections is defined. Cylindrical polar coordinates (r, ϕ, z) are used, and the inner and outer cylinders lie at $r = R_1$ and $r = R_2$ respectively. The inner cylinder rotates with angular velocity Ω_0 and the outer cylinder is at rest. When we refer to counter-rotating cylinder calculations, μ is the ratio of the outer to inner cylinder angular velocities. The radius ratio is $\eta = R_1/R_2$ and the gap between the cylinders is $R_2 - R_1 = d$.

The axisymmetric Navier–Stokes equations are

$$\boldsymbol{u}^0 \cdot \nabla \boldsymbol{u}^0 = -\frac{1}{\rho}\nabla p + \nu \nabla^2 \boldsymbol{u}^0, \tag{2.1}$$

$$\nabla \cdot \boldsymbol{u}^0 = 0, \tag{2.2}$$

with the boundary conditions u_r^0 and $u_z^0 = 0$ on $r = R_1$ and R_2, with $u_\phi^0 = 0$ on $r = R_2$ and $u_\phi^0 = \Omega_0 R_1$ on $r = R_1$. Also, $\boldsymbol{u}^0$ is periodic in the z-direction. These equations are solved for Taylor-vortex solutions which bifurcate from the Couette-flow solution, which has $\boldsymbol{u}^0 = (0, u_\phi^0, 0)$ at $Ta = Ta_c$. The corresponding Reynolds number is Re_c. The axial wavenumber α giving smallest Ta is nearly equal to π, so the corresponding cells are nearly square: the motion is assumed periodic in the axial direction with wavelength $\lambda = 2\pi/\alpha$. λ is then approximately $2d$, and corresponds to the length of a cell pair: we denote the cell size, $\frac{1}{2}\lambda$, by l. In experiments, the cylinders are of finite length, and so have an aspect ratio $\Gamma = h/d$, where h is the cylinder length. The theoretical results described here assume the limit $\Gamma \to \infty$, i.e. perfect spatial periodicity.

The rotation rate is expressed in dimensionless terms either by

$$Re = \Omega_0 R_1 d/\nu,$$

where ν is the kinematic viscosity, or by

$$Ta = 2\Omega_0^2 d^4 \eta^2 / \nu^2 (1-\eta^2),$$

so $Ta = 2(1-\eta)\,Re^2/(1+\eta)$. We denote the point of bifurcation from steady two-dimensional flow to time-dependent wavy flow by Ta_w or Re_w.

The numerical technique used to solve the nonlinear axisymmetric Taylor-vortex flow was a fully spectral method; the stream function ψ is defined so that the velocity $\boldsymbol{u}$ has components $[(-1/r)\,(\partial\psi/\partial z),\ u_\phi^0,\ (1/r)\,(\partial\psi/\partial r)]$ and is expanded as

$$\psi = \sum_{n=1}^{N} \sum_{m=0}^{M} \psi^{mn} T_m^*(x) \sin n\alpha z, \tag{2.3}$$

where $x = (r - R_1)/(R_2 - R_1)$ and T_m^* is the mth Chebyshev polynomial defined on the interval $[0, 1]$. Then u_ϕ^0 is similarly expanded as

$$u_\phi^0 = u_0(x) + \sum_{n=0}^{N} \sum_{m=0}^{M} v^{mn} T_m^*(x) \cos n\alpha z, \tag{2.4}$$

where $u_0(x)$ is the purely azimuthal Couette-flow solution of the Navier–Stokes equations. Although the series for ψ and u_ϕ^0 are truncated, the coefficients ψ^{mn} and v^{mn} can be chosen so that the Navier–Stokes equations are satisfied exactly at a number of selected collocation points: this gives rise to a set of nonlinear algebraic

equations which can be solved for these coefficients. Details of the procedure are given in Jones (1984).

Non-axisymmetric perturbations satisfy

$$\frac{\partial \boldsymbol{u}'}{\partial t} + \boldsymbol{u}^0 \cdot \nabla \boldsymbol{u}' + \boldsymbol{u}' \cdot \nabla \boldsymbol{u}^0 = -\frac{1}{\rho} \nabla p' + \nu \nabla^2 \boldsymbol{u}', \tag{2.5}$$

$$\nabla \cdot \boldsymbol{u}' = 0, \tag{2.6}$$

with boundary conditions $\boldsymbol{u}' = 0$ at $r = R_1$ and $r = R_2$. We take the time-dependence as $\exp[(\sigma - \mathrm{i}\omega)t]$ and the ϕ dependence as $\exp(\mathrm{i}m\phi)$, so that m is the (integer) azimuthal wavenumber. We regard m as an input parameter and solve for the eigenvalue $\sigma - \mathrm{i}\omega$. We usually work with the dimensionless wavespeed $c = \omega/m\Omega_0$, which is the ratio of the angular velocity of the waves to the angular velocity of the inner cylinder, rather than with ω itself. We assume that the perturbations have the same wavelength as the mean flow, but by a device described later we can accommodate perturbations whose wavelength λ is an integer multiple of the mean-flow wavenumber.

Only the out-of-phase wavy modes have been investigated: these modes have $u_r' = u_\phi' = \partial u_z'/\partial z = 0$ at the inflow and outflow boundaries where $u_z^0 = 0$.

The essential advance extending the range of Taylor number beyond the $Ta = 24000$ limit in Jones (1981) has been achieved by using finite differences in one direction and a spectral expansion in the other. Details are given in Jones (1984). The methods used here extend the range of Ta within computational reach to about 150000 or about $8Re_c$. The Taylor-vortex calculations used up to 16 horizontal Chebyshev modes and up to 14 vertical Fourier modes; the perturbations used NX = 16 horizontal Chebyshev modes and up to NZ = 61 vertical mesh points. The calculations were done on an IBM 370/168 at Newcastle University.

3. The stability boundary

In figure 1 we show the boundary for the onset of waviness in the (Ta, η)-plane. The neutral curves are shown for $m = 1, 2$ and 3; the neutral curves for higher m on this plane are omitted. Also shown is the neutral curve for the onset of axisymmetric Taylor vortices (Roberts 1965). This diagram extends the range of Taylor number covered in Jones (1981) by a factor of 5. The calculations for this diagram have used $\alpha = 3.13$, corresponding to approximately square cells. The experiments are in general agreement with figure 1, but unless the value of α is controlled by some means there is considerable scatter in the results for the wavy onset. Also, although many of the experiments have used long aspect ratios (e.g. Γ generally greater than 40), there are considerable variations in the different experimental set-ups. Despite these differences, it is clear that there is agreement generally between the experiments and the calculations (e.g. Cole 1981, 1983; Park & Jeong 1984; Zarti & Mobbs 1979).

Only the envelope of the calculated neutral curves can be compared directly with experiment, because at boundaries inside the envelope axisymmetric flows are unstable. Nevertheless, it is interesting to note that the lower-branch $m = 2$ mode and the $m = 1$ mode both become stable as Ta is increased. It is therefore not surprising that, in the experiments with narrow gaps, modes with increasing m are seen as the Taylor number is increased (Donnelly *et al.* 1979). The experiments also indicate that eventually this trend reverses as the Taylor number is further increased, and the lower values of m become favoured. This is consistent with the calculations here showing a second destablization of the $m = 2$ mode at higher values of Ta.

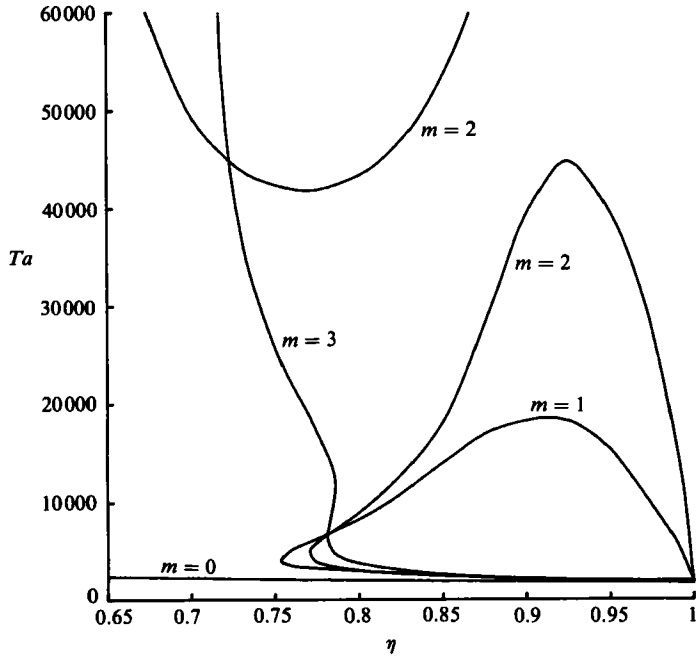

FIGURE 1. The $m = 0$ curve is the stability boundary for the onset of axisymmetric Taylor vortices. The curves $m = 1, 2$ and 3 are curves of neutral stability for the bifurcation from Taylor vortices. Curves for m greater than 3 are omitted. The axial wavenumber is $\alpha = 3.13$.

We also note that in a small range of η it is possible for waves with one wavenumber m to become unstable, then to restabilize, and then to become unstable again to an $m = 3$ mode as the Taylor number is increased. This unusual transition sequence has been observed recently by Park (1984) at $\eta = 0.782$.

In figure 2 we show the stability boundary in the plane $(\eta, Re/Re_c)$. This is the picture which can be compared most easily with experiment, as it is generally easier to determine the ratio of Re_w to Re_c than to find an absolute value (Cole 1983).

The other information which comes out of the eigenvalue problem is the wavespeed of the neutrally stable waves at the stability boundary. Wavespeeds are generally straightforward to measure experimentally, but difficulties occur if the waves are very weak, as they naturally are near the stability boundaries. It is of course possible to compare the speeds of unstable waves with the speeds of nonlinear waves, and this was done by Jones (1981, 1982). These predictions have not been uniformly successful. When the outer cylinder is at rest, the predictions have generally been within 5 % of the observed values (e.g. King *et al.* 1982; Ahlers, Cannell & Dominguez Lerma 1983). This error is much greater than experimental errors. The situation appears to be worse in the counter-rotating case, when $\mu < 0$ (Andereck, Liu & Swinney 1984). It is believed that the source of the error is the neglect of the nonlinearities of the waves; to reach the high standard of accuracy set by the experiments some account must be taken of these nonlinearities. It seems more sensible to wait for the development of theories which include the nonlinearities of the waves themselves before making detailed calculations. However, the agreement between theory and experiment for wavespeeds in the vicinity of the stability boundary is good even in the counter-rotating case (Andereck, Liu & Swinney 1984), and restricting our attention to this boundary still allows us to explore the dominant effects on wavespeeds.

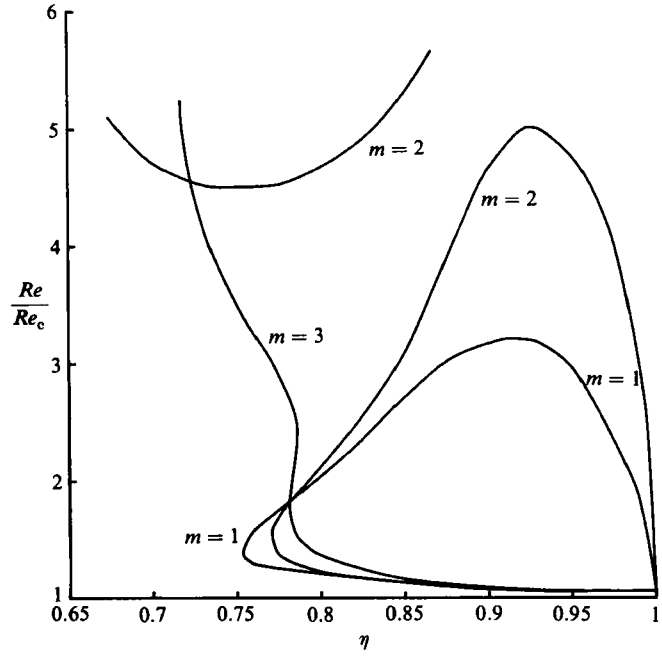

FIGURE 2. As for figure 1, but the ordinate is now Re/Re_c instead of Ta.

In figure 3 we show the wavespeed $c = \omega/m\Omega_0$ as a function of radius ratio for the modes $m = 1, 2$ and 3. The two branches of the $m = 2$ mode are labelled upper and lower according to their location in figure 1. Also shown on figure 3, for comparison, are the wavespeeds of the $m = 1, 2$ and 3 modes as they bifurcate from the Couette-flow solution. These bifurcations are never seen in practice when $\mu = 0$ because axisymmetric Taylor vortices occur at lower Taylor number. Nevertheless, we shall refer to them in §4 when we discuss the physical mechanisms involved in forming wavy vortices.

The general trends revealed in figure 3 are well known to experimentalists (e.g. Cole 1983; Lorenzen *et al.* 1983; King *et al.* 1982). The wavespeed is approximately 0.5 for narrow gaps at low Taylor numbers, and falls to much lower values as η is reduced, and falls more gently as Ta is increased, as can be seen by comparing values of the wavespeed for the different branches of the neutral curves.

The separate branches of the $m = 2$ curve raises the question of whether the two branches correspond to the same mode or two different modes. On the face of it, since the branches are not topologically connected it would seem they should be classified as distinct modes: however, a more careful analysis indicates that this is not appropriate. At fixed Ta, α, m and η, there is an infinite number of different eigenvalues; the great majority of these are very stable, corresponding to motions strongly damped by viscosity. If we vary Ta and η, keeping the other parameters fixed, we can trace these eigenvalues as we move from one part of the (Ta, η)-plane to another. We can then imagine surfaces covering the (Ta, η)-plane whose height corresponds to the real part of these eigenvalues. The point is that it is the same surface which is responsible for both the $m = 2$ neutral stability boundaries. In the region between these boundaries where the $m = 2$ mode is stable, this surface dips just below zero. All the unstable wavy modes found in this work are thus connected

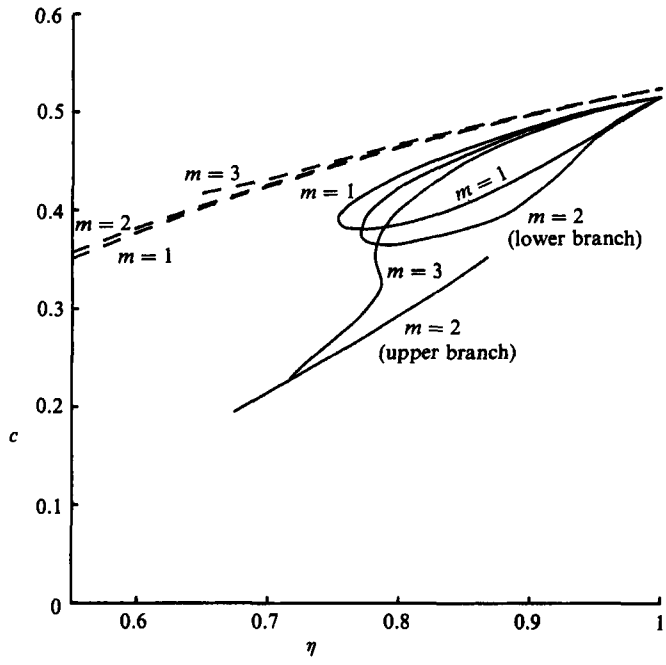

FIGURE 3. The wavespeed $c = \omega/m\Omega_0$ is plotted against radius ratio η, for $\alpha = 3.13$. The dashed curves are values for the bifurcation from azimuthal Couette flow; the solid curves are values for the bifurcation from Taylor vortices. When the curves have several values of c for one value of η, the lower value of c is always associated with the higher value of Ta_w.

with the classical narrow-gap wavy mode investigated by Davey *et al.* (1968), except for the jet modes discussed below.

Further evidence on the nature of the two branches of the $m = 2$ mode can be obtained by examining the eigenfunctions corresponding to points close to the neutral stability curve. In figure 4(*a*) we show the eigenfunctions associated with the $m = 2$ mode at $Ta = 48000$, $\eta = 0.84$ and $\alpha = 3.13$. This corresponds to a point in figure 1 near the lower branch of the $m = 2$ curve; in figure 4(*b*) the eigenfunctions are shown for a point near the upper branch, at $Ta = 60000$, $\eta = 0.68$ and $\alpha = 3.13$. The eigenfunctions are not identical, of course, but they show a strong similarity indicating that no dramatic change in character has occurred in passing from one branch to the other. We should note, however, that the phase speeds for these two waves are rather different: in case (*a*) the phase speed is 0.330 but in case (*b*) it is only 0.198. As we argue below, this substantial difference is due more to the change in the structure of the axisymmetric mean flow than to changes in the linearized eigenfunctions.

Eigenfunction pictures such as figures 4(*a*) and (*b*) must be interpreted with some care. To obtain the actually observed wavy flow pattern we have to add some small arbitrary multiple of these velocity flow patterns onto the basic axisymmetric flow. So in figures 4(*c*) and (*d*) we show the axisymmetric flows corresponding to figures 4(*a*) and (*b*) respectively. Similar pictures for this flow at different parameter values can be found in Jones (1981) and Fasel & Booz (1984). The eigenfunctions have a ϕ dependence, so that

$$u_r' = u_r^c(r,z)\cos m\phi + u_r^s(r,z)\sin m\phi,$$

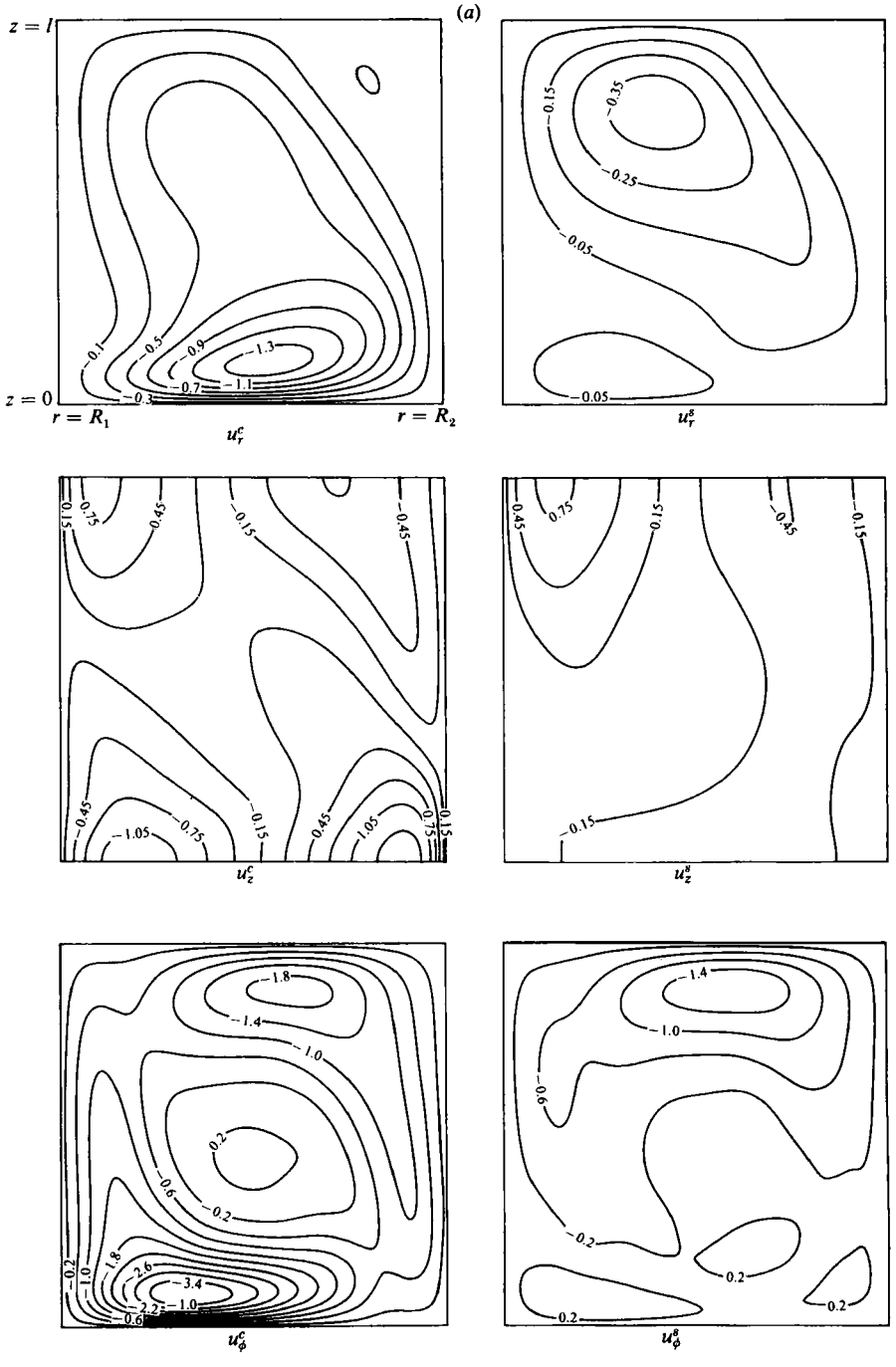

FIGURE 4(a). For caption see page 145.

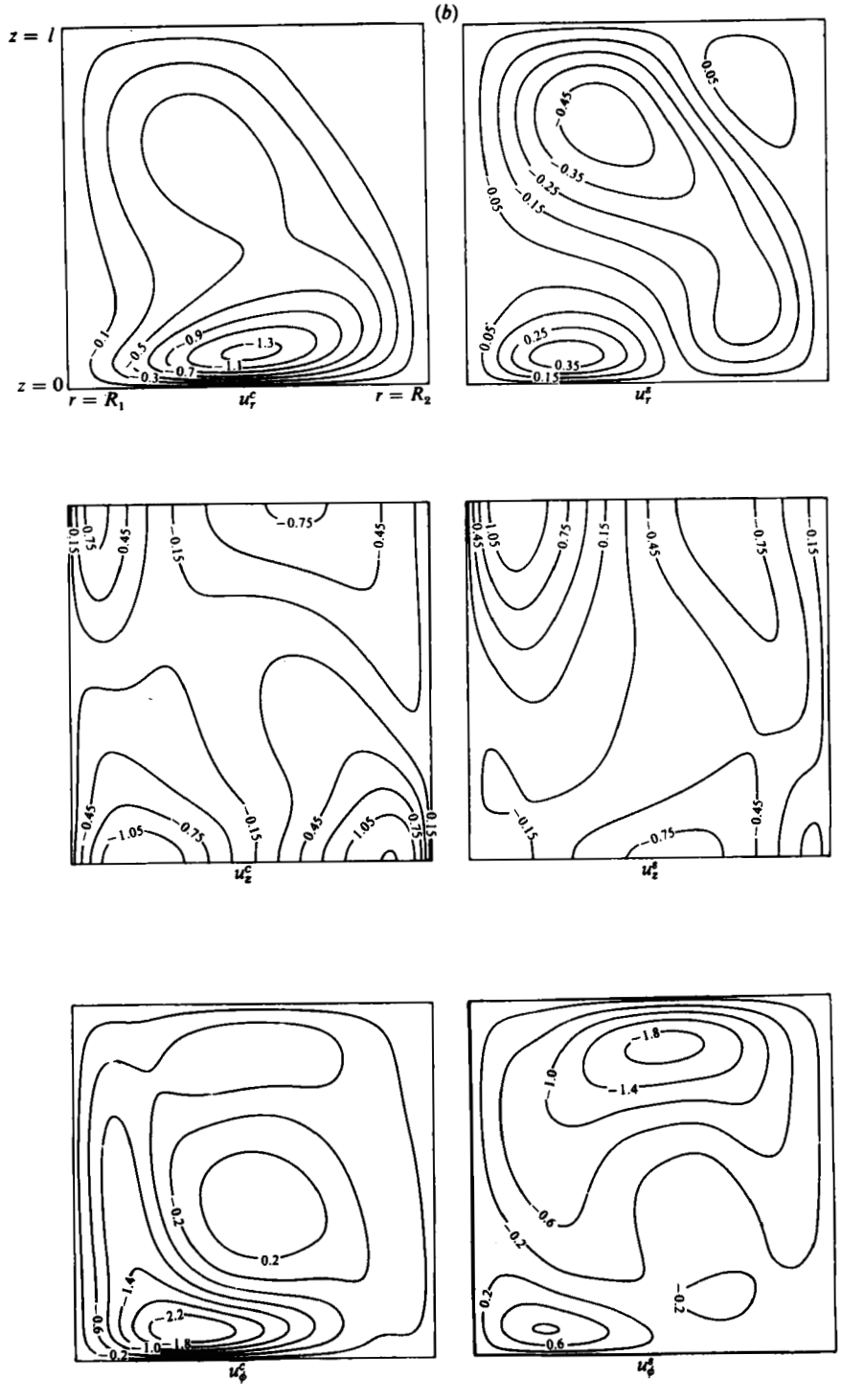

FIGURE 4(*b*). For caption see page 145.

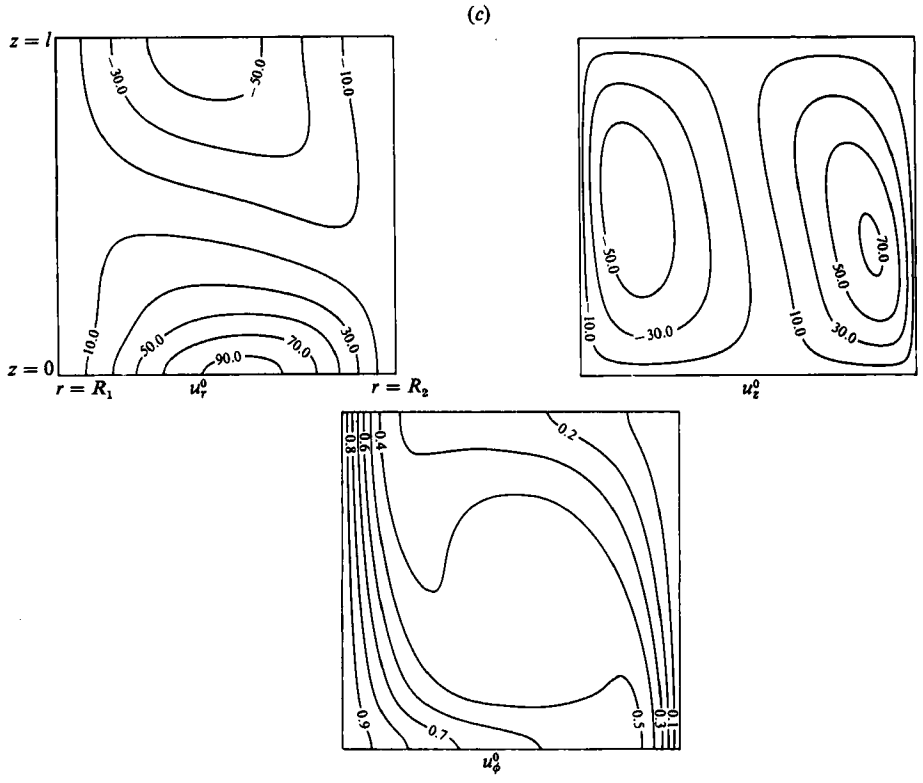

FIGURE 4(c). For caption see facing page.

and similarly for u_z' and u_ϕ'. An arbitrary phase factor is involved in where to choose $\phi = 0$; the choice made here is for $\phi = 0$ to coincide with the place where the wave has maximum amplitude near the outflow cell boundary, which is at $z = 0$ in these figures. The inflow cell boundary is then at $z = l$. To illustrate the difficulties of interpreting the eigenfunctions, we consider how the form of the wavy-outflow cell boundary would be found from figures 4(*a*) and (*c*). The wavy cell boundary, as observed in experiments, corresponds to the point where $u_z = 0$. At values of z just below $z = 0$ near the inner cylinder ($r = R_1$), the axisymmetric vortex velocity u_z^0 is positive (see figure 4*c* and recall that u_z^0 is antisymmetric about $z = 0$). Since the perturbation eigenfunction u_z^c is negative near here, the sum $u_z^0 + \epsilon u_z^c$ will be zero at some value of z just below $z = 0$. Near the outer cylinder ($r = R_2$), the axisymmetric vortex velocity u_z^0 is negative just below $z = 0$. But here the eigenfunction u_z^c is positive, so again the sum $u_z^0 + \epsilon u_z^c$ is zero at some value of z just below $z = 0$. Thus, although the perturbation u_z^c is positive when $z = 0$ near the inner cylinder and negative at $z = 0$ near the outer cylinder, nevertheless the wavy-outflow boundary is below $z = 0$ for all values of r at $\phi = 0$. Despite these difficulties, it is possible to work out the qualitative features of the wavy-vortex flow using these eigenfunctions.

Figures 1, 2 and 3 were all obtained for nearly square cells with $\alpha = 3.13$. We have also investigated how the wavy onset varies with α. The experiments of Mullin & Benjamin (1980), Lorenzen, Pfister & Mullin (1982), and Cole (1981, 1983) indicated that variations in aspect ratio strongly affected the onset of wavy vortices. From the work of Cole (1976) it was known that the onset of waviness is generally delayed by decreasing the aspect ratio and that the aspect ratio must be at least about 40 before this damping by the boundaries becomes small. The more recent observations

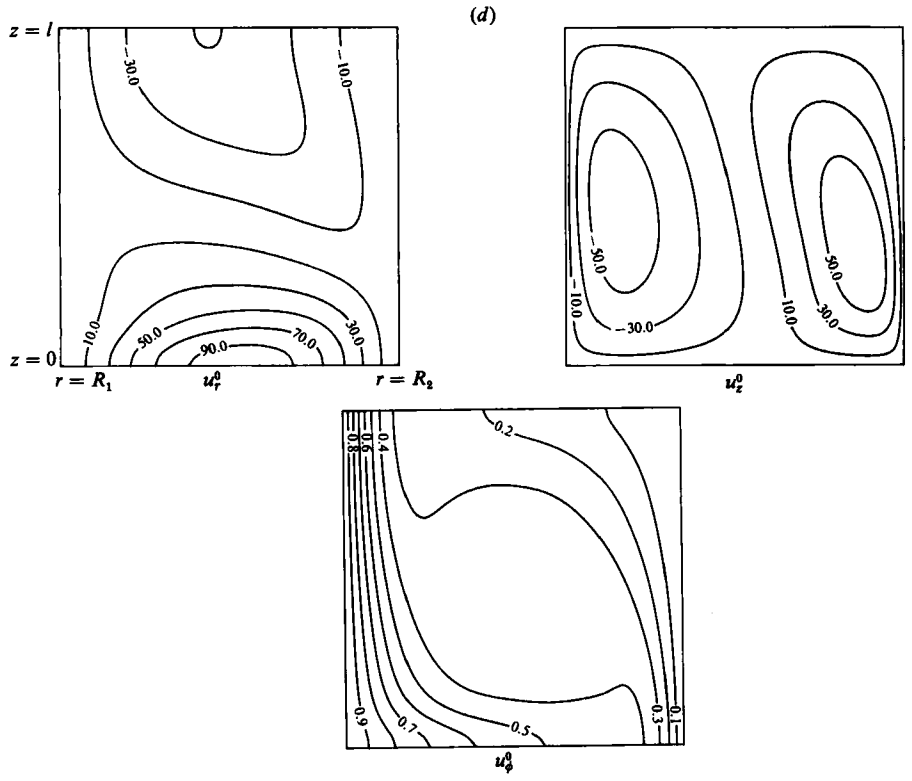

FIGURE 4(*a*), (*b*) Eigenfunctions of the classical wavy mode at $m = 2$ and $\alpha = 3.13$. Real and imaginary parts of the 3 velocity components are shown. The absolute amplitude is arbitrary, but for the relative amplitudes of the velocity components all velocities have been scaled on the viscous timescale: (*a*) $Ta = 48000$, $\eta = 0.84$; (*b*) $Ta = 60000$, $\eta = 0.68$. (*c*), (*d*) Contours of the axisymmetric Taylor vortex flow at $\alpha = 3.13$. Contours of the radial, axial and azimuthal velocity are shown. Radial and axial velocities are given in units of ν/d, but the azimuthal velocity is given in units of $\Omega_0 R_1$: (*c*) $Ta = 48000$, $\eta = 0.84$; (*d*) $Ta = 60000$, $\eta = 0.68$.

indicated, however, that quite small variations in aspect ratio could produce dramatic effects on wavy-vortex onset. Since these variations were produced by maintaining the number of cells in the apparatus fixed while the aspect ratio is adjusted (see e.g. Lorenzen *et al.* 1982) there are two possible reasons for this surprising result.

Firstly, it could be that the damping produced by the ends affects some modes very much more than others, or, secondly, it could be that the variations in cell size are responsible for the rapid variations in wavy critical Taylor number. If it is the second mechanism that is responsible, then the effect can be explained on the basis of infinite-cylinder calculations of the type done here: without some modelling of the endwalls we can do little about the first mechanism. The results of the calculations performed here indicate positively that it is the second mechanism which is dominant in producing the strong variations in Ta_w observed by Mullin & Benjamin (1980) and Lorenzen *et al.* (1982). Their striking results can therefore be understood (or at least reproduced by numerical calculations!) on the basis of the infinite-cylinder theory, by varying the parameter α. We can make no attempt to predict α theoretically: indeed, since it is well known experimentally that a wide range of different stable α-values can exist at the same value of the external parameters, such a theoretical prediction is clearly fraught with difficulty. The best that can be hoped for in the near future is to give bounds for the range of stable modes.

When the wavy-vortex boundary occurs at Taylor numbers close to critical, i.e. for narrow gaps, the dependence of Ta_w on α is similar to the dependence of Ta_c on α; a flat minimum when the cells are almost square, rising as α is either increased or decreased from 3.13. However, when the stability boundary occurs at values of Ta substantially above Ta_c, the behaviour is more interesting. The minimum critical Ta moves to values of α substantially less than 3.13, i.e. waves occur more easily in cells whose axial length is longer than d, their radial extent.

This behaviour is illustrated in figure 5(*a*). Here $\eta = 0.75$ and $\mu = 0$ and we plot Re/Re_c against cell size l/d. The solid curve is the numerically obtained stability boundary and the plotted points are the experimentally determined boundary given by Cole (1983). The agreement is quite remarkable, and deserves comment: first, the experiments are done with a very large aspect ratio of 65, so that damping by the end effects is small: secondly, there is some evidence that damping by the ends is more significant for the $m = 1$ mode and less significant for the higher-m modes such as $m = 3$: thirdly, the cell size in the experiments has been measured explicitly and the same value used in the calculations: fourthly, in order to get such good agreement the resolution in the numerical method has to be very high – 16 Chebyshev polynomials in the radial direction and 14 Fourier modes in the vertical direction were required for the axisymmetric Taylor-vortex solution and 16 radial modes with 41 vertical mesh points were needed in the perturbation calculation: see Jones (1984) for details.

The displacement of the point of minimum Ta_w to values of l/d well above 1 means that $\partial Ta/\partial\alpha$ is now quite significant near square-cell values with $l/d \approx 1$; experiments on the location of the Taylor-vortex boundary using approximately square cells will not be consistent unless l/d is carefully maintained at a constant value by some method. The experimental point near $\eta = 0.86$ has not been checked computationally because the cost of each run increases very rapidly as the Taylor number increases; this means it is not practical to follow the curve up to high values of the Reynolds number. However, the behaviour at lower Ta is consistent with the wavy-vortex boundary moving very rapidly upwards near $\eta = 0.86$.

The corresponding figure for the wave speeds is given in figure 5(*b*). The agreement with Cole's experiments is also quite good here, although the experimental scatter is greater, owing to the difficulty of measuring the speeds of very weak waves.

In figure 6 we have another comparison between the computations and Cole's experiments, this time at $\eta = 0.56$. Here the solid line is the best fit to the experimental data, and the crosses, circles and triangles are the computed points. The computations follow the trends of the experiments, but the computed values for the wavy-vortex mode at the large-l end of the figure, marked as triangles, are systematically lower than the experimental values. There seems to be little doubt that this is due to the damping of the waves by the endwalls; the aspect ratio for these experiments was 36, significantly less than for the $m = 3$ experiments noted earlier. The $m = 2$ mode was also examined in the vicinity of figure 6, but this is more stable than the $m = 1$ mode, in agreement with the observed preference for $m = 1$ at these values of η. In figure 7 we compare the experimental results of Lorenzen *et al.* (1982) with the computed values. Again the form of numerical and experimental curve is in general agreement, but here the stabilizing effect of the endwalls is even more marked, as the aspect ratio is lower than in Cole's apparatus.

The points computed with $l/d < 1$ correspond to eigenfunctions of a completely different character from the cases where $l/d > 1$. The branch found for $l/d > 1$ is the usual wavy mode, in the sense that it is topologically connected to the wavy mode

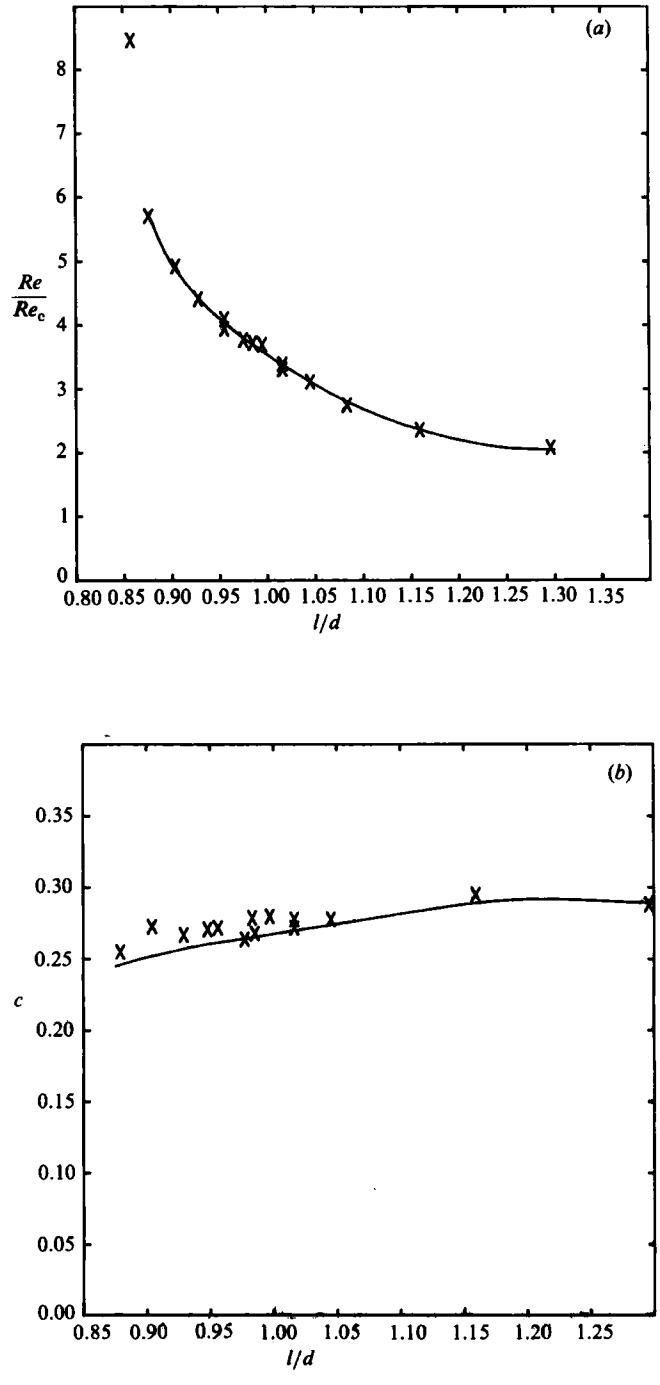

FIGURE 5. (*a*) Neutral stability curve in the plane (Re/Re_c, l/d), where l/d is the ratio of axial cell size to gap width, and (*b*) wavespeed $c = \omega/m\Omega_0$ at onset plotted against l/d. $m = 3$; $\eta = 0.75$; ——, the values from the computations; ×. experimental points of Cole (1983).

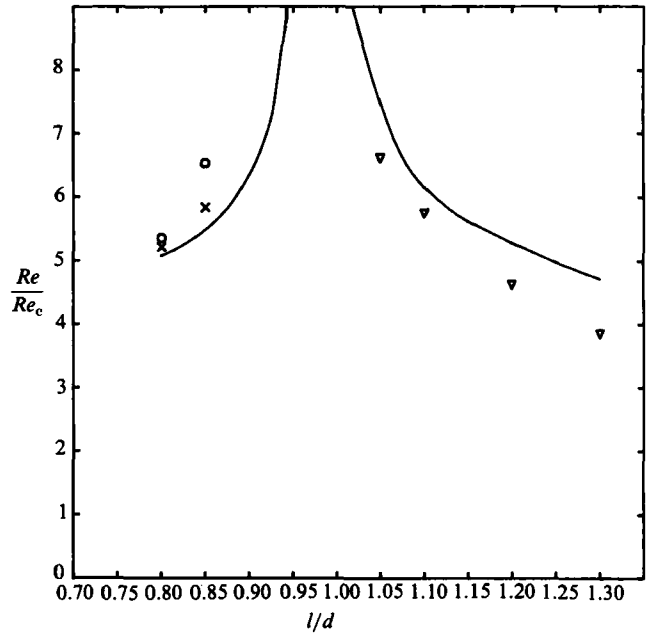

FIGURE 6. Neutral stability curves for $m = 1$ at $\eta = 0.56$, in the $(Re/Re_c, l/d)$-plane: ——, best fit through Cole's data; ▽, computed points for the classical wavy mode; ○, computed points for the harmonic jet mode; ×, computed points for the subharmonic jet mode. Points with l/d less than 1 refer to the jet modes: points with l/d greater than 1 refer to the usual wavy mode.

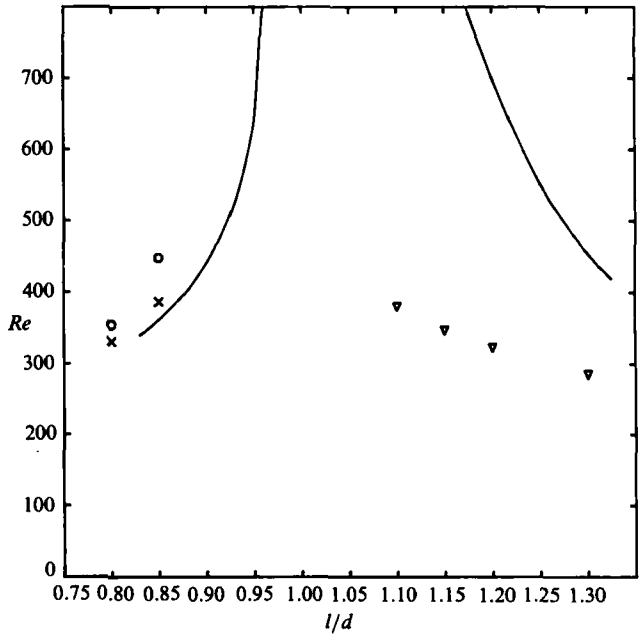

FIGURE 7. As for figure 6, but with $\eta = 0.507$, $m = 1$: ——, best fits through the low-aspect-ratio experiments of Lorenzen *et al.* and the computed points are labelled as in figure 6.

found theoretically by Davey *et al.* and found experimentally in narrow-gap apparatus. The wavespeed of this mode has dropped to only about 0.1 times the inner-cylinder speed when η has a value in the range 0.5–0.55. The modes occurring for $l/d < 1$ can be divided into two classes: both have greatest amplitude near the outflow cell boundary so we call them both jet modes, following the term coined by Lorenzen *et al.* (1982). One class of mode is subharmonic, with the axial wavelength of the perturbations twice the wavelength of the Taylor vortices. This mode is marked by crosses in figures 6 and 7. There can be little doubt that this computed mode corresponds to the jet mode found by Lorenzen *et al.* (1982) and by Cole (1983). They noted that, in the jet mode, adjacent outflow boundaries move in antiphase, which would be expected for a subharmonic mode of this type. Also, the wavespeeds of the subharmonic modes are consistent with the values given by Lorenzen *et al.* (1982) and are much greater than those found for the usual wavy modes. The wavespeeds of the computed points in figures 6 and 7 are given in table 1.

The circles in figures 7 and 8 correspond to a different mode, which we call the harmonic jet mode. Both the phase speed and stability boundary of the harmonic jet mode lie close to the values taken by the subharmonic jet mode, but the onset of the subharmonic jet mode is a little earlier than the harmonic jet mode, which presumably accounts for the subharmonic mode being the one seen in experiments. At the same value of Ta the harmonic jet mode has a phase speed slightly greater than that of the corresponding subharmonic jet mode.

In figure 8(*a*) we show the eigenfunctions corresponding to the subharmonic jet mode at $Ta = 80000$, $\eta = 0.56$, and $l/d = 0.8$. In figure 8(*b*) we give the eigenfunctions corresponding to the harmonic jet mode at the same parameter values. In order to help understand these pictures we also give the mean axisymmetric flow in figure 8(*c*). As noted in the discussion of figure 4, the interpretation of eigenfunctions requires some care. Two cells of the mean flow are shown, which accounts for the figures 8 having a length 1.6 times their width, although the cell length is only 0.8 of the cell width. Comparison of figures 8(*a*) and 8(*b*) sheds some light on the relationship between the subharmonic and harmonic jet modes. In both modes the amplitude in the vicinity of the inflow boundary is very small, and the behaviour of the subharmonic mode near $z = 2l/d$ is approximately that of the harmonic mode, but with the signs reversed. Experimentally we would therefore expect the subharmonic and harmonic jet modes to look very similar, but in the subharmonic case adjacent outflow boundaries are moving in antiphase, whereas in the harmonic case they move in phase. To obtain the subharmonic mode we have to make a slight modification of the usual procedure to take into account its subharmonic character. We first find the axisymmetric vortices corresponding to the wavelength $l/d < 1$ by the usual procedure, so that we have

$$\psi = \sum_{n=1}^{N} \sum_{m=0}^{M} \psi^{mn} T_m^*(x) \sin\left(\frac{2n\pi z}{\lambda}\right), \tag{3.1}$$

$$v = \sum_{n=0}^{N} \sum_{m=0}^{M} v^{mn} T_m^*(x) \cos\left(\frac{2n\pi z}{\lambda}\right). \tag{3.2}$$

We then convert this into a double-roll solution with wavelength $4l$ by the transformations $n \to (2n-1)$ in the ψ equation and $n \to 2n$ in the v equation. We then use the usual procedure to find the eigenvalues of disturbances with period $2l$. In order to keep the resolution in the z-direction approximately constant, more mesh points

η	Re	l/d	$\omega/m\Omega_0$	Type of mode
0.507	332	0.8	0.513	Subharmonic jet
0.507	387	0.85	0.497	Subharmonic jet
0.507	353	0.8	0.525	Harmonic jet
0.507	442	0.85	0.503	Harmonic jet
0.507	381	1.1	0.093	Classical wavy
0.507	350	1.15	0.098	Classical wavy
0.507	322	1.2	0.103	Classical wavy
0.507	285	1.3	0.112	Classical wavy
0.56	365	0.8	0.605	Subharmonic jet
0.56	406	0.85	0.592	Subharmonic jet
0.56	374	0.8	0.613	Harmonic jet
0.56	455	0.85	0.592	Harmonic jet
0.56	461	1.05	0.107	Classical wavy
0.56	399	1.1	0.116	Classical wavy
0.56	323	1.2	0.126	Classical wavy
0.56	271	1.3	0.136	Classical wavy

All modes here have $m = 1$.

TABLE 1. The phase speeds and critical Reynolds numbers are tabulated for the points computed for figures 6 and 7

are needed than for the standard wavy-mode calculations. NZ = 81 was used in the calculations here. Because of the numerical method used, CPU time increases only linearly with NZ (Jones 1984).

Lorenzen *et al.* also noted a mode in which the predominant motion is in the inflow boundary: this area has not yet been explored computationally. It may be seen from figures 6 and 7 that, whereas the wavy-mode computations all lie below the experimental curve, as we should expect if the endwalls are damping, for the jet, or subharmonic, mode the computations lie slightly above the experimental points. It is harder to resolve computationally the structure of the subharmonic mode as accurately as the wavy mode, so the results may not be as accurate for this mode as for the wavy mode: it is not yet clear whether this very small discrepancy is significant.

4. Physical mechanisms that make vortices wavy

The aim of this section is to present simple arguments that enable us to understand the shape of the neutral stability curves for the onset of wavy vortices. Since these neutral curves have a great deal of fine structure we clearly cannot expect more than the broad outlines of the behaviour from general arguments; detailed comparison with experiment requires accurate numerical calculation. Furthermore, the mechanisms we discuss here are based on consideration of the numerical work that has been done; there may well be new mechanisms at work in regions of the parameter space that are still unexplored, so the predictive power of the results in this section is likely to be quite limited. Nevertheless, provided they are used with great caution simple pictures can be useful.

We begin by formulating the energy integral for the perturbations to axisymmetric Taylor-vortex flow. We take the scalar product of the perturbation equation (2.5) with $\boldsymbol{u}'$; the viscous term can be rewritten using

$$\int_v \boldsymbol{u}' \cdot \nabla^2 \boldsymbol{u}' \, \mathrm{d}v = \int_v \nabla \cdot (\boldsymbol{u}' \wedge \boldsymbol{\omega}') \, \mathrm{d}v - \int_v \boldsymbol{\omega}' \cdot \boldsymbol{\omega}' \, \mathrm{d}v, \tag{4.1}$$

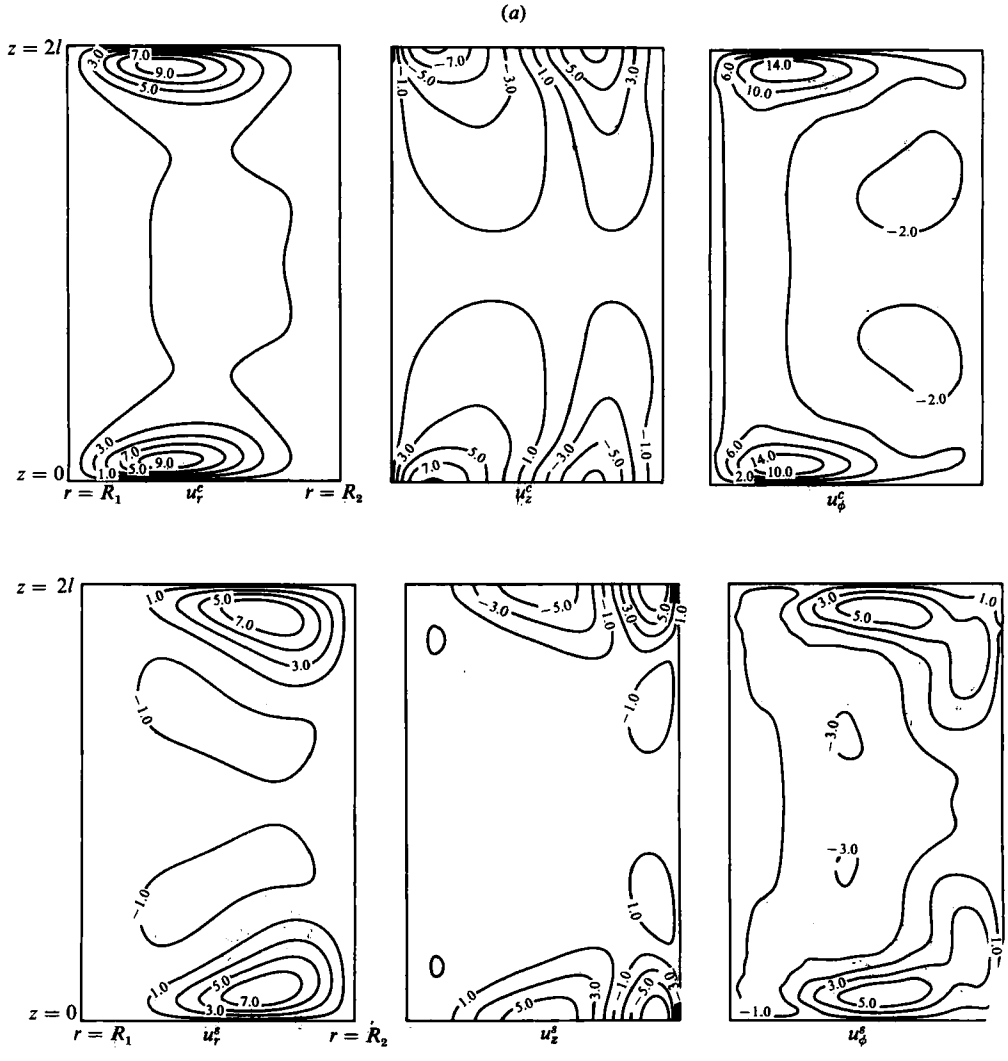

FIGURE 8(*a*). For caption see page 153.

where the divergence integral vanishes because of the boundary conditions. Then on substituting the form of the perturbations,

$$u_r' = \tfrac{1}{2}(u_r'(r,z)\,\mathrm{e}^{\mathrm{i}m\phi}\,\mathrm{e}^{(\sigma-\mathrm{i}\omega)t} + u_r'^{*}(r,z)\,\mathrm{e}^{-\mathrm{i}m\phi}\,\mathrm{e}^{(\sigma+\mathrm{i}\omega)t}), \tag{4.2}$$

and similarly for the ϕ and z components, we can divide the resulting energy integral into 5 component parts, each of which has a simple interpretation:

$$\sigma E_1 + E_2 + E_3 + E_4 = E_5, \tag{4.3a}$$

$$E_1 = \int (u_r' u_r'^{*} + u_z' u_z'^{*} + u_\phi' u_\phi'^{*})\,\mathrm{d}v, \tag{4.3b}$$

$$E_2 = \int \left[\tfrac{1}{2}(u_r' u_\phi'^{*} + u_\phi' u_r'^{*})\left(\frac{\partial u_\phi^0}{\partial r} - \frac{u_\phi^0}{r}\right) + \frac{u_\phi' u_\phi'^{*} u_r^0}{r}\right]\mathrm{d}v, \tag{4.3c}$$

$$E_3 = \int \tfrac{1}{2}(u_z' u_\phi'^{*} + u_\phi' u_z'^{*})\frac{\partial u_\phi^0}{\partial z}\,\mathrm{d}v, \tag{4.3d}$$

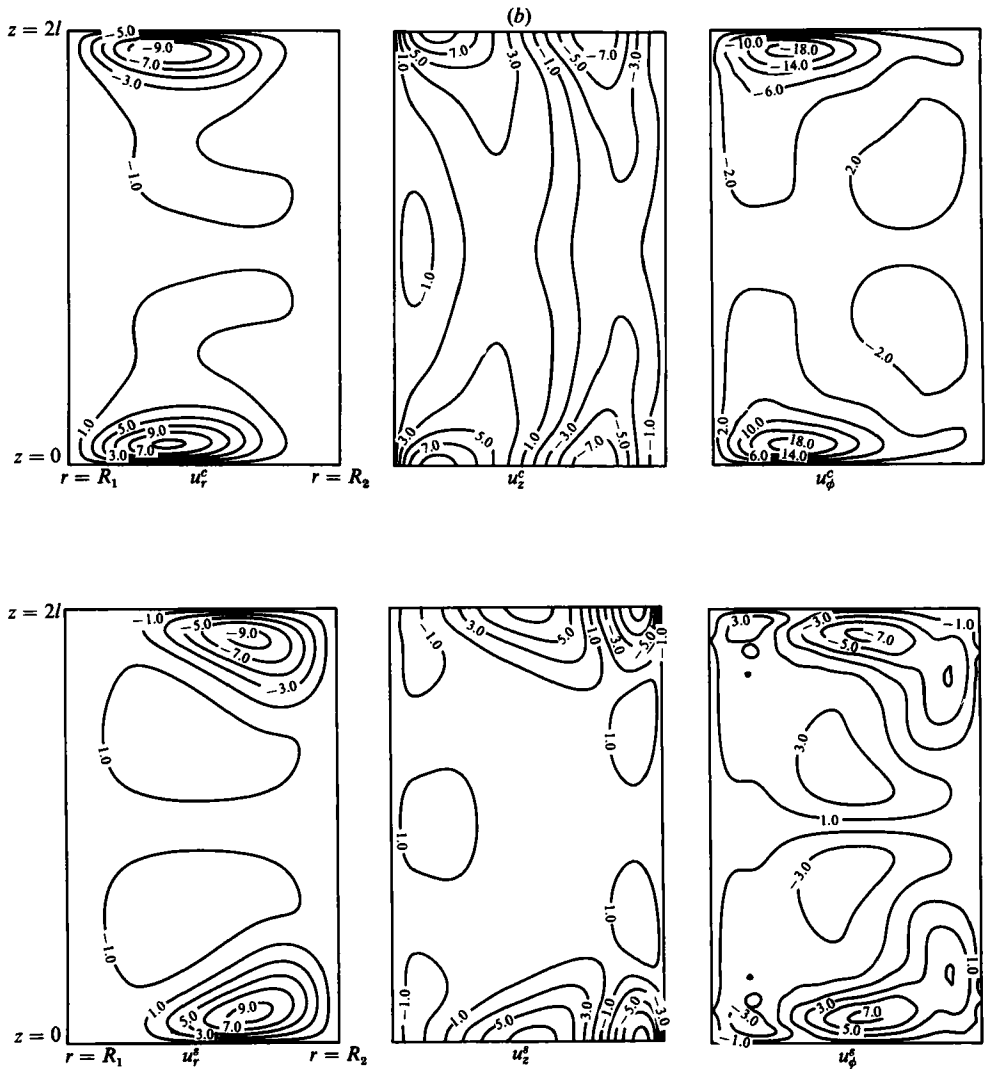

FIGURE 8(*b*). For caption see facing page.

$$E_4 = \int \left[u_r' u_r'^* \frac{\partial u_r^0}{\partial r} + \tfrac{1}{2}(u_r' u_z'^* + u_z' u_r'^*) \left(\frac{\partial u_r^0}{\partial z} + \frac{\partial u_z^0}{\partial r} \right) + u_z' u_z'^* \frac{\partial u_z^0}{\partial z} \right] \mathrm{d}v, \tag{4.3e}$$

$$E_5 = \int (\omega_r' \omega_r'^* + \omega_z' \omega_z'^* + \omega_\phi' \omega_\phi'^*) \, \mathrm{d}v. \tag{4.3f}$$

Here * denotes complex conjugate, and E_1 represents the kinetic energy of the disturbance: it grows when σ is positive and decays when it is negative. The neutral curve is therefore determined by the condition $E_2 + E_3 + E_4 = E_5$. E_5 represents viscous dissipation and is positive definite. In all the cases considered E_5 is the term of largest magnitude in the vicinity of a neutral mode. E_2, E_3 and E_4 represent the rate of working of the Reynolds stresses on the various shears which are present in the Taylor vortices. E_3 represents work done by the axial shear of the azimuthal velocity and E_4 represents work done by shears of the flow in the axial plane. This axial flow is considerably smaller than the azimuthal flow, so E_4 is neglected in the

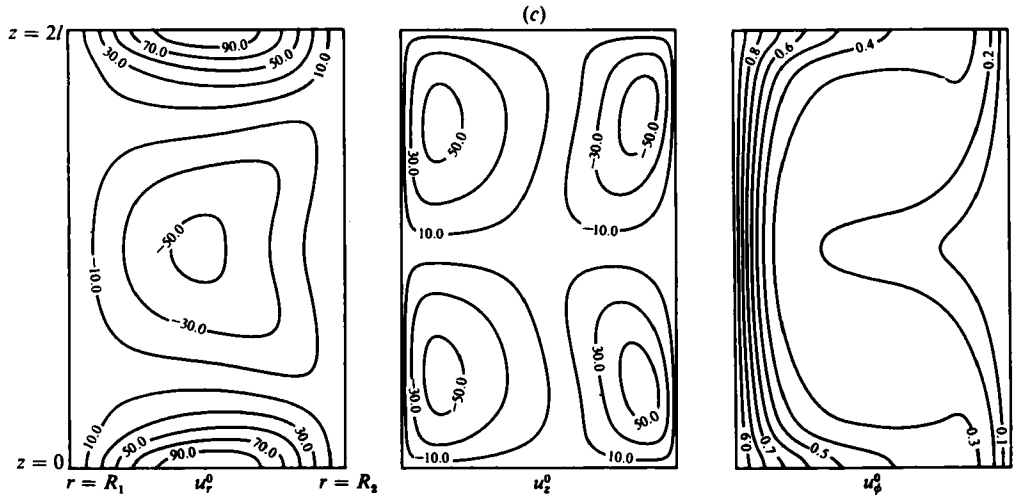

FIGURE 8. (*a*) Eigenfunctions for the subharmonic jet mode at $Ta = 80000$, $\eta = 0.56$, $l/d = 0.8$. Contours of the real and imaginary parts of the radial, axial and azimuthal velocity perturbations are shown. The components are scaled as in figure 4. (*b*) As in (*a*) but for the harmonic jet mode. (*c*) Contours of velocity of the axisymmetric Taylor-vortex flow at the parameter values of (*a*). Two cells of the flow are shown. Velocity components are scaled as in figure 4(*c*).

following discussion. We stress that this result is based on the numerical experience, which is limited to the regions of the parameter space we have investigated. E_2 is the rate of working of the radial shear of the azimuthal flow together with a centrifugal term. There seems to be no advantage in separating these two contributions.

If the mean flow is purely Couette flow, then E_3 and E_4 are zero so that the neutral stability curve is determined by the balance of E_2 and E_5. For narrow gaps Couette flow becomes unstable to non-axisymmetric disturbances for values of Ta only slightly greater than Ta_c. This can be seen in figure 9, where the neutral curves for the non-axisymmetric modes are shown in the (η, Ta)-plane for α fixed at 3.13. So, in the vicinity of Ta_c, $E_2 = E_5$. As pointed out by Meyer (1966, 1969) and Davey *et al.* (1968), the effect of the nonlinear Taylor vortices is to give $u_\phi^0(z)$ the profile of a jet in the neighbourhood of the inflow and outflow regions of the axial flow. In figure 10 we show contour plots for the azimuthal velocity u_ϕ^0 for a number of cases. In all the plots, contours of u_ϕ^0 are equally spaced with $u_\phi^0/\Omega_0 R_1 = 1$ at $r = R_1$ and $u_\phi^0 = 0$ at $r = R_2$. Cases (*a*), (*c*) and (*e*) are all for $\eta = 0.95$ (narrow gap) and have $Ta = 4000$, 60000 and 60000 respectively. The case (*c*) is for nearly square cells ($\alpha = 3.13$), but case (*e*) has $\alpha = 2.417$ ($l = 1.3d$). Cases (*b*), (*d*) and (*f*) have the same Ta and α values as the figures opposite but are for $\eta = 0.5$ (wide gap). In figure 11 we show the azimuthal velocity profiles at the value $r = \frac{1}{2}(R_1 + R_2)$. The diagrams in figure 11 show a full period of profile containing two cells. Various trends are apparent in figures 10 and 11. In cases (*a*) and (*b*), which are for low Taylor number, angular momentum is advected out in a broad region centred on the outflow cell boundary, and angular momentum is reduced in the neighbourhood of the inflow boundary. The profile of u_ϕ^0 in figure 11 is therefore roughly sinusoidal; but it is noticeable even at low Ta that the mean value of u_ϕ^0 in figure 11(*b*) is well below $0.5\Omega_0 R_1$. As the Taylor number is increased, the broad outflow and inflow regions are concentrated into internal boundary layers and the u_ϕ^0 profile is flat except for

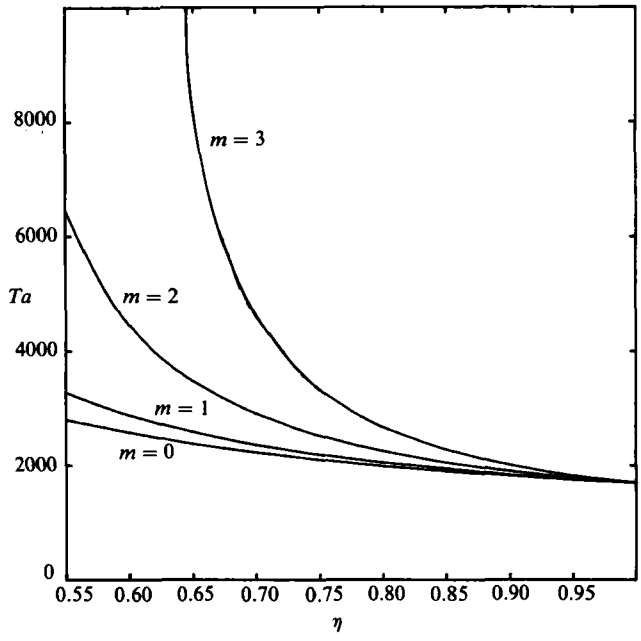

FIGURE 9. Neutral stability curves for the bifurcation from azimuthal Couette flow.

strong jets at the inflow and outflow cell boundaries. In the narrow-gap cases (*c*) and (*e*) the jets are fairly symmetrical, but in the wide-gap case there is a strong asymmetry; the outflow jet is concentrated into a narrow region, but the inflow jet is broader. It is also apparent that the mean azimuthal velocity for wide gaps and large Ta is well below $0.5\Omega_0 R_1$; a value nearer $0.2\Omega_0 R_1$ is indicated for the parameters of cases (*d*) and (*f*). It is important to distinguish these jets in the azimuthal direction from the jets in the axial plane: although the azimuthal jets are created by the axial ones, the actual flow velocity in the axial plane is smaller than the azimuthal flow, which is why the E_3 term is more important than the E_4 term. It is the azimuthal jets which destabilize the axisymmetric flow; since there is already a near balance between E_2 and E_5 for narrow gaps, very little is required from E_3 to make the vortices wavy. In consequence, the onset of wavy vortices occurs close to the onset of axisymmetric vortices for narrow gaps. From figure 9 we can see that the near balance between E_2 and E_5 for non-axisymmetric modes near Ta_c no longer holds for wide gaps. The onset of Couette flow to non-axisymmetric modes occurs at much higher Ta than instability to the $m = 0$ mode. This is not surprising; in the narrow-gap case an $m = 1$ mode corresponds to an azimuthal wavelength of about $\pi(R_1 + R_2)$, which is much greater than $2d$, the approximate wavelength in the axial and radial directions. So for narrow gaps the viscous dissipation, which is proportional to $(k_r^2 + k_\phi^2 + k_z^2)$, is approximately proportional to $(k_r^2 + k_z^2)$. But for wide gaps the ratio $2d/(R_1 + R_2)$ is no longer small, so the viscous dissipation is increased. In consequence, the E_3 term has to do much more in the wide-gap case than in the narrow-gap case to make up the difference between E_2 and E_5. So the onset of waviness is delayed to higher Taylor numbers.

The above argument, although it does explain the major feature of the delay in onset of waviness at wide gaps, leaves many questions unanswered. Why is the rise so sudden at $\eta = 0.75$? Why does the $m = 2$ curve have two branches? Why is $m = 1$

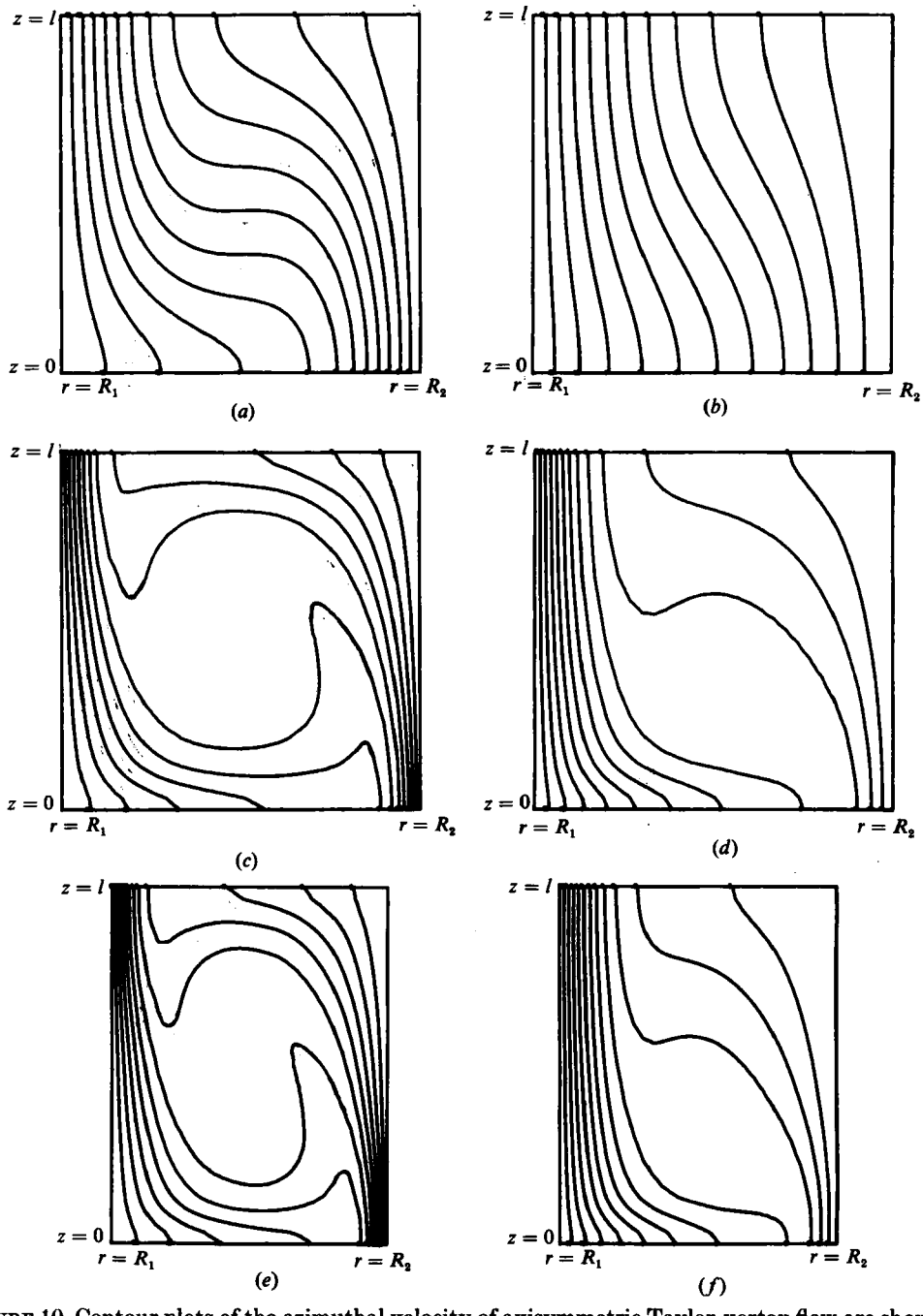

FIGURE 10. Contour plots of the azimuthal velocity of axisymmetric Taylor-vortex flow are shown. The contours are equally spaced. (*a*) $\eta = 0.95$, $Ta = 4000$, $\alpha = 3.13$. (*b*) 0.5, 4000, 3.13. (*c*) 0.95, 60000, 3.13. (*d*) 0.5, 60000, 3.13. (*e*) 0.95, 60000, 2.417. (*f*) 0.5, 60000, 2.417.

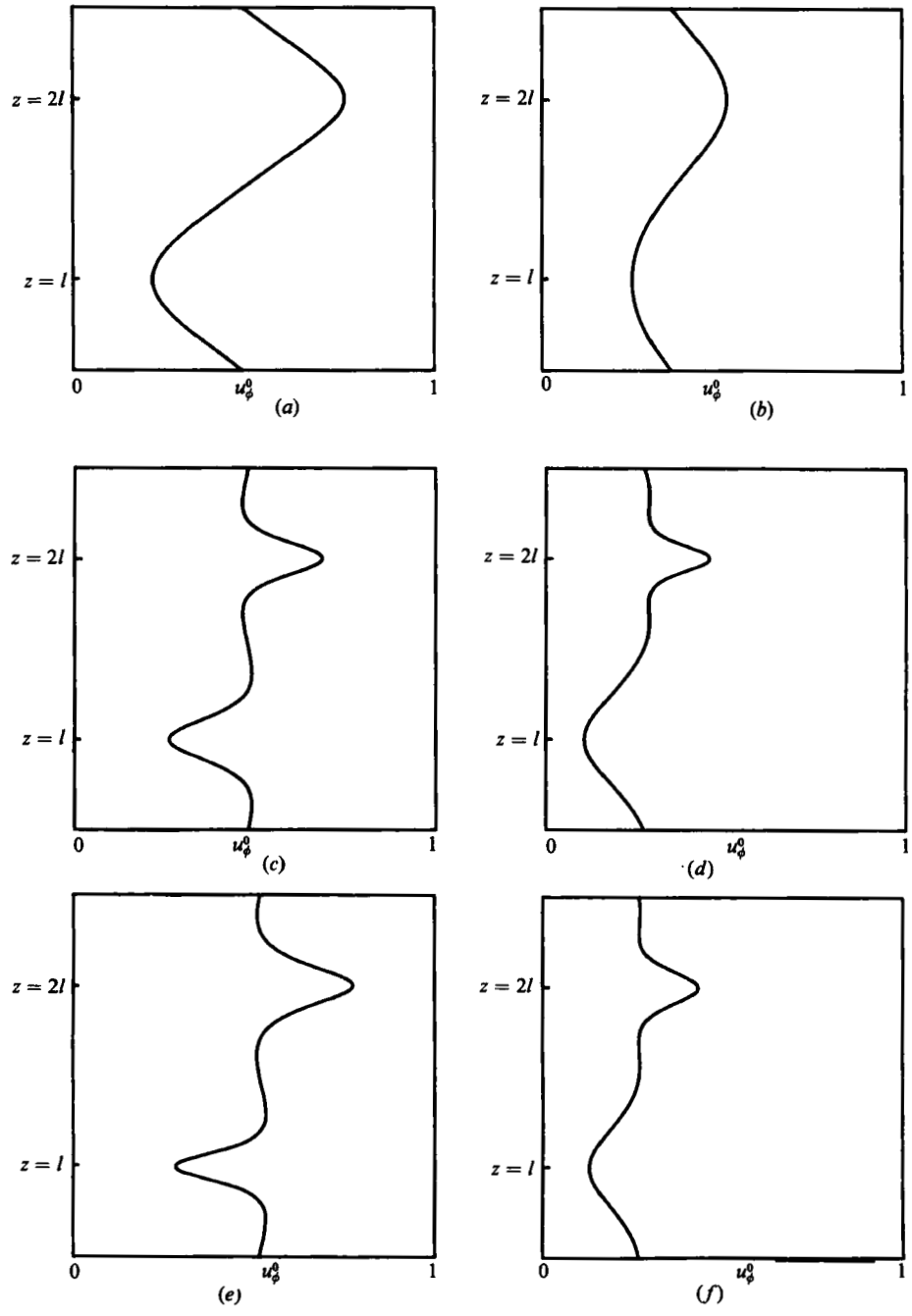

FIGURE 11. Velocity profiles $u_\phi^0(z)$ at $r = \frac{1}{2}(R_1 + R_2)$. The parameter values correspond to those in figure 10.

seen at $\eta < 0.6$ and $\eta > 0.8$ but not in between? Finally, why does the wavespeed fall so rapidly as the gap becomes wider? To answer these questions we need to examine the behaviour of the energy integrals as Ta and η are varied.

We illustrate typical behaviour in figures 12(*a*) and (*b*); here we show E_2/E_5 and E_3/E_5 as functions of Ta for $\eta = 0.8$ (case *a*) and $\eta = 0.95$ (case *b*), with $m = 2$, both

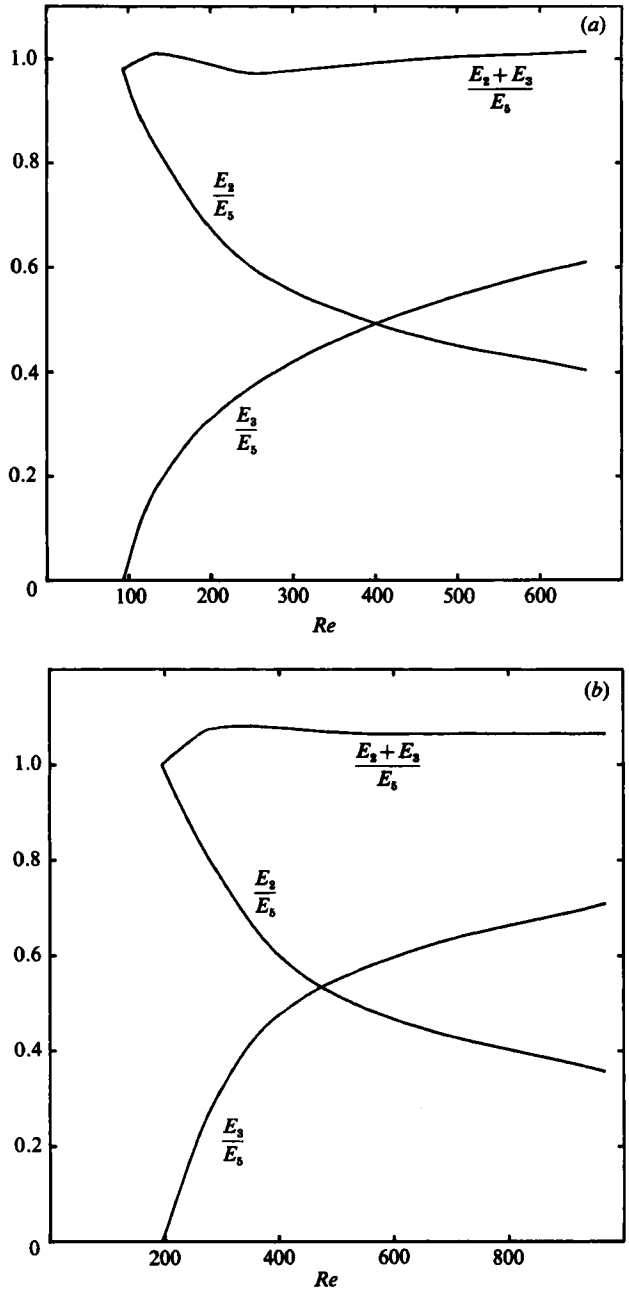

FIGURE 12. E_2/E_5, E_3/E_5 and $(E_2+E_3)/E_5$ are plotted against Re for $m = 2$, $\eta = 0.8$, $\alpha = 3.13$. (*a*) $\eta = 0.8$, (*b*) 0.95.

with $\alpha = 3.13$. E_4/E_5 is less than 1 % throughout the range of figure 12, so we ignore it. The sum $(E_2+E_3)/E_5$ can be seen to hover near 1 in case (*a*), sometimes falling below, giving stability, and sometimes rising above, giving instability. This compensation effect is why the rise in Ta_w is so rapid in the neighbourhood of $\eta = 0.77$; since $(E_2+E_3)/E_5$ is very insensitive to Ta, stability depends primarily on the η-value. Thus, in the narrow-gap case (*b*), the sum $(E_2+E_3)/E_5$ is also very flat, but here the value it hovers near is 1.06, safely into the unstable regime.

The decline in E_2/E_5 as Ta is increased seems odd at first sight: as Ta is increased, the inner-cylinder speed increases as $Ta^{\frac{1}{2}}$ relative to the viscous decay time, so the radial shear also increases. This increase is, however, more than compensated for by the concentration of the radial gradient of velocity into boundary layers. Batchelor (1960) gives an asymptotic argument that the boundary-layer thickness at the inner and outer cylinder walls is $\delta \sim Ta^{-\frac{1}{4}}$. Although we are not strictly in the large-Ta asymptotic regime, this result nevertheless does give some insight into figure 12: since the term $r\,\partial(u_\phi^0/r)/\partial r$ is only large in the boundary layers, where it is $O(\delta^{-3})$, the integral is small because $(u_r' u_\phi'^* + u_r'^* u_\phi')$ is small there. In fact, if we assume that the shape of the eigenfunctions is unchanged with increasing Ta, $(u_r' u_\phi'^* + u_r'^* u_\phi')$ will be $O(\delta^3)$, and so the contribution to E_2 will be only $O(\delta)$. If we assume the form of the eigenfunctions can be changed as Ta increases, it is then possible, by choosing eigenfunctions which peak in the boundary layer, to make $E_2/E_5 \sim Ta^{-\frac{1}{4}}$: such modes would become unstable at large Ta, and may be connected with the 'herring bone' modes discussed by Barcilon *et al.* (1979). This happens at much higher Ta than is discussed here.

This concentration of the mean-velocity gradient into boundary layers is due to the nonlinear development of the Taylor vortices. This is the mechanism by which the Taylor vortices suppress competing modes and hence retain their coherent character far beyond Ta_c. Similar behaviour occurs in the Bénard convection problem.

We now consider the variation of E_3 with Ta and η. E_3 is zero at the onset of Taylor vortices, and increases monotonically as Ta is raised. However, it does flatten out at higher Ta.

For more detailed behaviour of E_3, we briefly consider the stability of an inviscid jet corresponding to the axial shear of the azimuthal flow, as recommended in Davey *et al.* (1968). Since viscosity is important in the real flow, results must be interpreted with great care. We consider two simple models of jets: model A has a mean flow $u(z)$ in the x-direction given by

$$\left.\begin{aligned} u(z) &= 0, \quad z < -a, \\ u(z) &= \frac{u_0(z+a)}{a}, \quad -a < z < 0, \\ u(z) &= \frac{u_0(a-z)}{a}, \quad 0 < z < a, \\ u(z) &= 0, \quad z > a, \end{aligned}\right\} \tag{4.4}$$

and models the azimuthal velocity profile in the neighbourhood of an inflow or outflow boundary. Model B has a periodic mean flow given by

$$\left.\begin{aligned} u(z) &= \frac{u_0(a-z)}{a}, \quad 4na < z < 2a+4na, \\ u(z) &= \frac{u_0(z+a)}{a}, \quad 4na-2a < z < 4na, \end{aligned}\right\} \tag{4.5}$$

for all integer n.

In either case, the disturbance stream function satisfies Rayleigh's equation (Rayleigh 1880)

$$(u-c)(D^2-k^2)\psi - \psi \frac{\mathrm{d}^2 u}{\mathrm{d}z^2} = 0, \tag{4.6}$$

with ψ and $(u-c)\,\mathrm{d}\psi/\mathrm{d}z - \psi\,\mathrm{d}u/\mathrm{d}z$ continuous across the jumps in $\mathrm{d}u/\mathrm{d}z$. The

wavespeed is the real part of c, c_r, and the growth rate $\sigma = kc_i$ where c_i is the imaginary part of c. Then, in model A,

$$\left.\begin{aligned} c_r &= \frac{u_0[2ak-1-\exp(-2ak)]}{ak}, \\ \sigma &= \frac{u_0\{16\exp(-2ak)-[2ak-3-\exp(-2ak)]^2\}^{\frac{1}{2}}}{4a}. \end{aligned}\right\} \tag{4.7}$$

When the term inside the square root is negative, the corresponding disturbance is stable: this must always be the case for k sufficiently large; in this case $k_{\max} = 1.8327/a$. Maximum growth rate occurs for k somewhat less than this value, $k = 1.2258/a$. The small-k expansions are

$$c_r \sim \frac{u_0 ak}{2}, \quad \sigma \sim u_0\left(\frac{ak^3}{3}\right)^{\frac{1}{2}}, \tag{4.8}$$

so the growth rate is non-zero, but tends to zero for long waves.

The corresponding results in model B are

$$c_r = 0, \quad \sigma = u_0\{2ak\coth 2ak - 1 - a^2k^2\}^{\frac{1}{2}}. \tag{4.9}$$

Again, when the term inside the square root is negative, we have stability. In this case the large-k cut-off is at $k_{\max} = 1.1997/a$ and maximum growth rate is when $k = 0.8031/a$. The small-k expansion is

$$c_r = 0, \quad \sigma \sim \frac{u_0 k}{\sqrt{3}}. \tag{4.10}$$

In the circular geometry of Couette flow, $k \approx 2m/(R_1+R_2) = 2(1-\eta)\,m/d(1+\eta)$. For square cells, the axial period is $2d$, so we let $a = \frac{1}{2}d$ in model B. The maximum growth rate is then when $(1-\eta)\,m \approx 0.8(1+\eta)$; for $\eta = 0.875$ this gives $m = 12$, whereas for $\eta = 0.6$ this gives $m \simeq 3$. In practice, the observed wavenumbers are lower than this, probably owing to viscosity damping out higher-m modes more strongly than lower m modes. We are therefore operating in the long-wavelength region of the shear instability mechanism where (4.8) and (4.10) are relevant. In this region, $\sigma \sim m^{\frac{1}{2}}$ and m in models A and B respectively. The shear-flow mechanism would like to move to higher azimuthal wavenumber: in regions where viscosity damps out higher wavenumbers strongly, such as $\eta \simeq 0.6$ or lower (see figure 9) the tendency is suppressed, but at $0.7 < \eta < 0.8$ this tendency emerges, and $m = 2$ and $m = 3$ are preferred to $m = 1$. For narrow gaps this tendency manifests itself in the dominance of larger-m modes at moderate Taylor numbers; but the onset of waves in narrow gaps is so close to Ta_c that the shear flow component is dominated by E_2, and $m = 1$ is preferred at onset.

These models also indicate why wavelengths longer than $2d$ are preferred by the wavy-mode instability at $\eta \leqslant 0.8$. The jet is then quite narrow, since Ta_w is then much larger than Ta_c, so model A is preferred to model B. In model A σ increases with a, so longer axial wavelengths are preferred.

We now turn to the problem of the reduced wavespeeds as η decreases. From figure 3 we can see that the wavespeeds fall as η decreases, even in the neighbourhood of the bifurcation from Couette flow. This can be explained simply in geometrical terms; because the radius of the outer cylinder is larger there is more slow-moving fluid than fast-moving fluid; the azimuthal velocity averaged over the fluid is less than $\frac{1}{2}\Omega_0$. However, this effect is small compared to the drop in wavespeed

occurring as the waves bifurcate from the Taylor vortices. When $\eta = 0.5$, the wavespeeds can be as low as 0.1 times the inner-cylinder angular speed. For values of η as low as this, there is a strong asymmetry between the jets at the outflow and inflow boundaries (see figures 11*d* and *f*). From these pictures it is clear that the jet near the outflow boundary is much narrower than that at the inflow boundary (see also Fasel & Booz 1984). Also, the mean azimuthal velocity is well below $0.5\Omega_0 R_1$; for the cases here a value of near $0.2\Omega_0 R_1$ is indicated. However, even this effect does not seem sufficient to reduce wavespeeds to the very low values found. We might naïvely expect that since the outflow-jet region has higher velocity gradients than the inflow jet it would do the bulk of the driving. However, the result in (4.8) indicates the exact opposite. The growth rate increases as a increases, despite the fact that the shear falls as a increases. We also note that increasing a brings the wavespeed c nearer to the velocity in the centre of the jet. We therefore suggest that the bulk of the driving comes from the inflow jet, and that the wavespeed is dominated by the fluid speed in the neighbourhood of the inflow jet, which is much lower than the 'mean' azimuthal velocity. We should not forget, perhaps, that, even for the $m = 1$ mode at $\eta = 0.56$, nearly half the driving comes from the E_2 terms, so that, whereas the above arguments may indicate the reasons behind the trends, they cannot give the whole picture.

5. Conclusions

The main conclusion we draw from these calculations is that the infinite-cylinder model is capable of describing the complex behaviour of the transition to wavy vortices reasonably well. All the major features of the model, and even some of the rather detailed predictions, have been seen experimentally. Thus the bend in the (Re, η)-plane (figure 2) in the neighbourhood of $\eta = 0.78$ implies that the waves should die out as the Reynolds number is increased, and then reappear as an $m = 3$ wave at higher values of the Reynolds number: this unusual transition sequence has been observed by Park (1984) at $\eta = 0.782$. The major features are the move to smaller values of m as the preferred mode as η is reduced below 0.8 and the emergence of strong dependence on the cell wavelength, the move to very low wavespeeds for the wavy mode as η is reduced down to 0.5, and the appearance of the jet modes; these features have all been seen in a variety of different experiments. The only jet mode reported so far is the subharmonic mode; it will be of interest to see if the harmonic jet mode can be detected experimentally.

The effects of the ends on the transition to wavy vortices enter in two ways: first, they control the axial wavelength, although not uniquely in a long-aspect-ratio apparatus; secondly, the ends provide some damping, delaying the onset of waves to higher values of the Reynolds number.

The first effect, that on axial wavelength, can be treated in the infinite-cylinder approximation by regarding axial wavelength as an external parameter which is not determined theoretically but must be measured by experiment. Since it is the variation in axial wavelength that produces most of the interesting effects observed by Lorenzen *et al.* (1982), it follows that these phenomena can be treated with the infinite-cylinder theory. In some apparatus, such as that of King & Swinney (1983), fluid can be added or removed while the cylinders are running, allowing the axial wavelength to be directly controlled. In a more conventional apparatus, though, the axial wavelength selected depends on the route taken to achieve the state, and is subject to certain quantization conditions (Park & Donnelly 1981) depending on how

many cells are to be fitted in. The experiments indicate that many different states are possible at the same value of parameters such as the Reynolds number (e.g. Mullin & Benjamin 1980). If the route taken to a particular value of Re is that of slow ramping from a low-Re state, then the final axial wavenumber may be generally unique (Park & Crawford 1983). All this information is gathered from experiments, however; all we can do from theoretical considerations is to impose rather broad limits on the values of the axial wavelength that are linearly stable (Kogelman & DiPrima 1970).

The second effect of the ends is to provide a damping on the wavy mode. This effect cannot be discussed in the infinite-cylinder approximation, and can only be estimated by examining the departures of experimental results from the theoretical values given here. The damping of the wavy mode is considerable if the aspect ratio is less than about 30, as can be seen from figures 6 and 7. The evidence suggests, however, that, if the aspect ratio is greater than 50, the agreement between theory and experiment becomes good, indicating that the theoretical infinite-cylinder values are approached as the aspect ratio becomes large. The subharmonic jet mode appears to be much less affected by the ends than the classical wavy mode. For the wavy mode, simple models of the type proposed by Walgraef, Borckmans & Dewel (1983) may be adequate to obtain the correction terms for long, but finite, cylinders.

I am grateful to Dr Alan Cole and to Professor K. Park for access to unpublished experimental results, and also for many helpful conversations.

REFERENCES

AHLERS, G., CANNELL, D. S. & DOMINGUEZ LERMA 1983 Possible mechanism for transitions in wavy Taylor-vortex flow. *Phys. Rev.* A **27**, 1225–1227.

ANDERECK, C. D., LIU, S. S. & SWINNEY, H. L. 1984 *Flow Regimes in a Circular Couette System with Independently Rotating Cylinders.* Univ. of Texas Preprint.

BARCILON, A., BRINDLEY, J., LESSEN, M. & MOBBS, F. R. 1979 Marginal stability in Taylor–Couette flows at very high Taylor number. *J. Fluid Mech.* **94**, 453–463.

BATCHELOR, G. K. 1960 Appendix to an empirical torque relation for supercritical flow between rotating cylinders (by R. J. Donnelly & N. J. Simon). *J. Fluid Mech.* **7**, 416–418.

COLE, J. A. 1976 Taylor vortex instability and annulus length effects. *J. Fluid Mech.* **75**, 1–15.

COLE, J. A. 1981 Wavy vortex onset and cylinder radius ratio. In *Proc. 2nd Taylor vortex flow working party, Tufts University*, pp. 11–12. Tufts University, Medford, Mass.

COLE, J. A. 1983 The effect of cylinder radius ratio on wavy vortex onset. In *Proc. 3rd Taylor vortex flow working party* (Nancy) pp. 1–4.

DAVEY, A., DIPRIMA, R. C. & STUART, J. T. 1968 On the instability of Taylor vortices. *J. Fluid Mech.* **31**, 17–52.

DIPRIMA, R. C., EAGLES, P. M. & NG, B. S. 1984 The effect of radius ratio on the stability of Couette flow and Taylor vortex flow. To appear in *Phys. Fluids.*

DONNELLY, R. J., PARK, K., SHAW, R. & WALDEN, R. W. 1979 Early non-periodic transitions in Couette flow. *Phys. Rev. Lett.* **44**, 987–989.

EAGLES, P. M. 1971 On stability of Taylor vortices by fifth-order amplitude expansions. *J. Fluid Mech.* **49**, 529–550.

FASEL, H. & BOOZ, O. 1984 Numerical investigation of supercritical Taylor-vortex flow for a wide gap. *J. Fluid Mech.* **138**, 21–52.

JONES, C. A. 1981 Nonlinear Taylor vortices and their stability. *J. Fluid Mech.* **102**, 249–261.

JONES, C. A. 1982 On flow between counter-rotating cylinders. *J. Fluid Mech.* **120**, 433–450.

JONES, C. A. 1984 Numerical methods for the transition to wavy Taylor vortices. To appear in *J. Comp. Phys.*

KING, G. P., LI, Y., LEE, W., SWINNEY, H. L. & MARCUS, P. S. 1982 Wave speeds in wavy Taylor vortex flow. *J. Fluid Mech.* **141**, 365–390.

KING, G. P. & SWINNEY, H. L. 1983 Limits of stability and irregular flow patterns in wavy vortex flow. *Phys. Rev.* A **27**, 1240–1243.

KOGELMAN, S. & DIPRIMA, R. C. 1970 Stability of spatially periodic supercritical flows in hydrodynamics. *Phys. Fluids* **13**, 1–11.

LORENZEN, A., PFISTER, G. & MULLIN, T. 1982 End effects on the transition to time-dependent motion in the Taylor experiment. *Phys. Fluids* **26**, 10–13.

MEYER, K. 1966 A two-dimensional time-dependent numerical study of rotational Couette flow. *Los Alamos rep.* LA-3497, Los Alamos, New Mexico.

MEYER, K. 1969 Three-dimensional study of flow between concentric rotating cylinders. In High Speed Computing in Fluid-Dynamics. *Phys. Fluid Suppl.* II **12**, 165–170.

MULLIN, T. & BENJAMIN, T. B. 1980 Transition to oscillatory motion in the Taylor experiment. *Nature* **288**, 567–569.

PARK, K. 1984 Unusual transition in Taylor wavy vortex flow. *Phys. Rev.* A **29**, 3458–3460.

PARK, K. & CRAWFORD, G. L. 1983 Deterministic transitions in Taylor wavy-vortex flow. *Phys. Rev. Lett.* **50**, 343–346.

PARK, K. & DONNELLY, R. J. 1981 Study of the transition to Taylor vortex flow. *Phys. Rev.* A **24**, 2277–2279.

PARK, K. & JEONG, K. 1984 Stability boundary of Taylor vortex flow. Submitted to *Phys Fluids.*

RAYLEIGH, LORD 1880 On the stability, or instability, of certain fluid motions. *Proc. Lond. Math. Soc.* **11**, 57–70.

ROBERTS, P. H. 1965 Appendix to 'Experiments on the stability of viscous flow between rotating cylinders' (by R. J. Donnelly & K. W. Schwarz). *Proc. R. Soc. Lond.* A **283**, 531–556.

TAYLOR, G. I. 1923 Stability of a viscous liquid contained between two rotating cylinders. *Phil. Trans. R. Soc. Lond.* A **223**, 289–343.

WALGRAEF, D., BORCKMANS, P. & DEWEL, G. 1983 Onset of wavy Taylor vortex flow in finite geometries. *Phys Rev.* A **28**.

ZARTI, A. S. & MOBBS, F. R. 1979 Wavy Taylor vortex flow between eccentric rotating cylinders. Energy conservation through fluid film lubrication technology: Frontiers in Research and Design. ASME publications.